Geophys. J. Int. (201x) **xxx**, 1–**??**

Supporting Information

Marion Y. Thomas[1] and Harsha S. Bhat[2]

[1]*Department of Earth Sciences, University of Oxford, Oxford, UK*
South Parks Road Oxford OX1 3AN, UK ; mthomas.tectonics@gmail.com
[2]*Laboratoire de Géologie, Ecole Normale Supérieure, CNRS- UMR 8538, PSL Research University, Paris, France*
24 rue Lhomond, Paris, France ; harsha.bhat@ens.fr

16 July 2018

The following supporting information provide the equations used to build the damage constitutive model. An extended description of the model can be found in Bhat et al. (2012); Perol & Bhat (2016) and Thomas et al. (2017). The different parameters and constants used for the constitutive model are summarized in Table S1.

S1 CONTRIBUTION OF MICROCRACKS

S1.1 Gibbs free energy of a damage solid

Our model defines the constitutive stress-strain relationship in terms of Gibbs free energy ($W^G = W^{G_e} + W^{G_i}$), using an energy-based approach. The elastic strain energy density is given by:

$$W^{G_e}(\boldsymbol{\sigma}) = \frac{1}{4\mu}\left[2\tau^2 + \frac{3(1-2\nu)}{(1+\nu)}\sigma^2\right] \tag{s1}$$

where μ is the shear modulus, ν the Poisson's ratio, and ρ the mass density. Then, since all cracks in our model have the same orientation, the Gibbs function associated with inelastic deformation at constant $\boldsymbol{\sigma}$ can be written in terms of the Gibbs free energy per crack $\Delta W^G(\boldsymbol{\sigma}, D)$ time the number of crack per unit volume (N_v):

$$W^{G_i}(\boldsymbol{\sigma}, D) = N_v \Delta W^G(\boldsymbol{\sigma}, D) \tag{s2}$$

The Gibbs free energy per crack depends on the fracture energy release rate G (crack growth) and the surface energy γ_s (to create a surface):

$$\Delta W^G(\boldsymbol{\sigma}, D) = \int_o^{\Gamma} \left[G(\boldsymbol{\sigma}, D) - 2\gamma_s\right] \mathrm{d}s \tag{s3}$$

where $\mathrm{d}s$ describes the position along the micro-crack and Γ corresponds to the locus of all crack fronts. Based on fracture mechanics, for an isotropic elastic solid, the energy release rate G can be related to the stress intensity factors at the tip of the crack by:

$$G(\boldsymbol{\sigma}, D) = \frac{1-\nu^2}{E}\left[K_I^2(\boldsymbol{\sigma}, D) + K_{II}^2(\boldsymbol{\sigma}, D) + \frac{K_{III}^2(\boldsymbol{\sigma}, D)}{(1-\nu)}\right] \tag{s4}$$

Where E is the Young's modulus. However, under dynamic loading rates, the wing cracks quickly quite Mode II and Mode III to become purely tensile. As a consequence their contributions are neglected in this model and the total Gibbs free energy of the damages solid can be approximated as:

$$W^G(\boldsymbol{\sigma}, D) = W^{G_e}(\boldsymbol{\sigma}) + N_v \int_{\Gamma}\left[\frac{1-\nu^2}{E}K_I^2(\boldsymbol{\sigma}, D) - 2\gamma_s\right] \mathrm{d}s \tag{s5}$$

S1.2 Evaluating the stress intensity factors K_I at the tip of the crack.

To compute the stress intensity factor K_I, the state of stress needs to be evaluated on each penny cracks. To generalize the problem the normal stress is represented by the first invariant of the stress tensor and the shear stress by the second invariant of the deviatoric stress tensor (see equation 8).

Under **Regime I** (compressive loading) stresses are not high enough to allow sliding or opening of the microcraks. Hence, the solid is assumed to behave like an isotropic linear elastic solid and therefore $W^{G_i}(\boldsymbol{\sigma}, D)$ is assumed to be zero.

Under **Regime II** (compressive loading), the Mode-I stress intensity factor K_I^{R-II} has 3 main contributions. (1) The frictional sliding on the initial flaws in the rocks (penny shaped cracks in the model) creates a wedging force F_w that acts on the wing crack faces. F_w corresponds to the component of the sliding force, resolved normal to the direction of the most compressive stress $\sigma 1$:

$$F_w = (\tau + f\sigma)\,\pi a^2 \sin\Phi \tag{s6}$$

(2) The second component takes into account the interaction between micro-cracks as they grow. The wedging force F_w induces a tensile stress $\sigma^{(i)}$ on neighboring wing-cracks, that increases as they get closer to each-other. Following Ashby & Sammis (1990) and Bhat et al. (2012), $\sigma^{(i)}$ is defined by:

$$\sigma^{(i)} = \frac{F_w}{A_{crk} - \pi\left(l + \alpha a\right)^2} \quad \text{with} \quad A_{crk} = \pi^{1/3}\left(\frac{3}{4N_v}\right)^{2/3} \tag{s7}$$

where A_{crk} represents the average area occupied per crack and $\pi\left(l + \alpha a\right)^2$ is the total crack area projected parallel to $\sigma 1$. (3) Finally, as expected under compressive regime, the remote confining stress, characterized by σ, tends to close the wing cracks. Consequently, for **Regime II**, the Mode-I stress intensity factor for one crack in a loaded solid is given by:

$$K_I^{R-II} = \frac{F_w}{\left[\pi\left(l + \beta a\right)\right]^{3/2}} + \frac{2}{\pi}\left(\sigma + \sigma^{(i)}\right)\sqrt{\pi l} \tag{s8}$$

Factor $\beta(= 0.1)$ has been defined by Ashby & Sammis (1990) to give a limiting value of K_I when l meets zero. Then, since we assume an homogeneous isotropic distribution of pre-existing

flaws per unit volume, rewriting equation s8 in terms of D and D_0 corresponds to compute the effective stress intensity factor for a unit volume containing N_v cracks of size $(l + \alpha a)$:

$$K_I^{R-II}(\sigma, D) = \sqrt{\pi a_0}[A(D)\sigma + B(D)\tau] \tag{s9}$$

where:

$$A(D) = fc_1(D) + c_3(D)[fc_2(D) + 1] \tag{s10}$$
$$B(D) = c_1(D) + c_2(D)c_3(D) \tag{s11}$$

and

$$c_1(D) = \frac{\sqrt{1-\alpha^2}}{\pi\alpha^{3/2}[(D/D_0)^{1/3} - 1 + \beta/\alpha]^{3/2}} \tag{s12}$$
$$c_2(D) = \left(\frac{\sqrt{1-\alpha^2}}{\alpha}\right)\left(\frac{D_0^{2/3}}{1-D^{2/3}}\right) \tag{s13}$$
$$c_3(D) = \frac{2\sqrt{\alpha}}{\pi}[(D/D_0)^{1/3} - 1]^{1/2} \tag{s14}$$

Note that for D approaching 1, K_I^{R-II} tends to infinite, which actually illustrates the coalescence of the microcracks.

Regime III prevails under tensile loading: it induces opening of both penny shape and wing cracks. In that particular regime, following Budiansky & O'connell (1976) and Kachanov (1987), the stress intensity factor K_I^{R-III} is a quadratic function of the stress invariants:

$$K_I^{R-III}(\sigma, D) = \sqrt{\pi a_0}[C^2(D)\sigma^2 + O^2(D)\tau^2]^{1/2} \tag{s15}$$

with

$$C(D) = A + \Omega\sqrt{\alpha[D/D_0]^{1/3}} \tag{s16}$$
$$O(D) = \sqrt{\frac{B^2C^2}{C^2 - A^2}} \tag{s17}$$

C and O are determined by ensuring the continuity of conjugate strains between **Regime II** and **Regime III** (see section S3).

S2 DETERMINING THE CONSTITUTIVE STRESS-STRAIN RELATIONSHIP

S2.1 Constitutive relationship for Regime I

Under **Regime I**, there is no sliding or opening of the microcraks. Therefore the Gibbs free energy is given by:

$$W^G(\boldsymbol{\sigma}, D) = W^{G_e}(\boldsymbol{\sigma}) = \frac{1}{4\mu}\left[2\tau^2 + \frac{3(1-2\nu)}{(1+\nu)}\sigma^2\right] \tag{s18}$$

and the strain-stress relationship follows linear elasticity:

$$\sigma_{ij} = 2\mu\left[\epsilon_{ij} + \frac{\nu}{1-2\nu}\epsilon\delta_{ij}\right] = 2\mu\epsilon_{ij} + \lambda\epsilon\delta_{ij} \tag{s19}$$

where λ is the Lamé's first parameter.

S2.2 Constitutive relationship for Regime II

For **Regime II** and **III**, following equation s5, the Gibbs free energy can be written as the sum of the elastic contribution, $W^{G_e}(\boldsymbol{\sigma})$, and the inelastic contribution due to the presence of microcracks, $W^{G_i}(\boldsymbol{\sigma}, D)$ (see equation s5). Following Deshpande & Evans (2008) and Bhat et al. (2012), we assume that the constants A and B of K_I^{R-II} and C and O of K_I^{R-III} are only a function of the ratio l/a (and not l and a separately) and therefore we can treat them as constants. We thus find that the Gibbs free function for **Regime II** can be approximated by :

$$W^G(\boldsymbol{\sigma}, D) = W^{G_e}(\boldsymbol{\sigma}) + \frac{1}{4\mu}\left[A_1\sigma + B_1\tau\right]^2 \tag{s20}$$

where

$$A_1 = A\sqrt{\frac{\pi D_0(1-\nu)}{\alpha^3}} \quad \text{and} \quad B_1 = B\sqrt{\frac{\pi D_0(1-\nu)}{\alpha^3}}; \tag{s21}$$

If we express the above expression in term of conjugate strains invariants $\epsilon = \epsilon_{kk}$ and and $\gamma = \sqrt{2e_{ij}e_{ij}}$ with $e_{ij} = \epsilon_{ij} - 1/3\epsilon\delta ij$, we obtain the Helmotz free energy. Differentiating once $W^H(\boldsymbol{\epsilon}, D)$ with respect to strain we obtain the stress-strain relation:

$$\begin{aligned}\sigma_{ij} =& \frac{\mu}{\Gamma}\left\{\left(\frac{3(1-2\nu)}{(1+\nu)} + A_1^2 - \frac{A_1B_1\epsilon}{\gamma}\right)\epsilon_{ij}\right.\\ &\left. + \left(\frac{3\nu}{(1+\nu)} + \frac{B_1^2}{2} - \frac{A_1^2}{3} + \frac{A_1B_1\epsilon}{3\gamma}\right)\epsilon\delta_{ij} - \left(\frac{A_1B_1}{2}\right)\gamma\delta_{ij}\right\}\end{aligned} \tag{s22}$$

$$\text{with} \quad \Gamma = \left[\frac{3(1-2\nu)}{2(1+\nu)} + \frac{3(1-2\nu)B_1^2}{4(1+\nu)} + \frac{A_1^2}{2}\right] \tag{s23}$$

Based on equation s22 we can define the equivalent Lamé parameters μ^* and λ^*:

$$\mu^* = \frac{\mu}{2\Gamma}\left(\frac{3(1-2\nu)}{(1+\nu)} + A_1^2\right) \quad \text{and} \quad \lambda^* = \frac{\mu}{\Gamma}\left(\frac{3\nu}{(1+\nu)} + \frac{B_1^2}{2} - \frac{A_1^2}{3}\right) \tag{s24}$$

and therefore approximate the change in waves speed occurring in the medium:

$$c_p^* = \sqrt{\frac{\lambda^* + 2\mu^*}{\rho}} \quad \text{and} \quad c_s^* = \sqrt{\frac{\mu^*}{\rho}} \tag{s25}$$

S2.3 Constitutive relationship for Regime III

Under **Regime III**, the Gibbs free energy is given by:

$$W^G(\boldsymbol{\sigma}, D) = W^{G_e} + \frac{1}{4\mu}\left[C_1^2\sigma^2 + O_1^2\tau^2\right] \tag{s26}$$

where

$$C_1 = C\sqrt{\frac{\pi D_0(1-\nu)}{\alpha^3}} \quad \text{and} \quad O_1 = O\sqrt{\frac{\pi D_0(1-\nu)}{\alpha^3}}; \tag{s27}$$

Differentiating the Helmotz free energy with respect to strain gives the constitutive relationship:

$$\sigma_{ij} = \mu\left\{\left(\frac{4}{2+O_1^2}\right)\epsilon_{ij} + \left(\frac{2}{\frac{3(1-2\nu)}{(1+\nu)} + C_1^2} - \frac{4}{3[O_1^2+2]}\right)\epsilon\delta_{ij}\right\} \tag{s28}$$

Following the same logic as for **Regime II** we can define the equivalent Lamé parameters μ^* and λ^* to compute the change in waves speed occurring in the medium:

$$\mu^* = \mu\left(\frac{2}{2+O_1^2}\right) \quad \text{and} \quad \lambda^* = \mu\left(\frac{2}{\frac{3(1-2\nu)}{(1+\nu)} + C_1^2} - \frac{4}{3[O_1^2+2]}\right) \tag{s29}$$

S3 CRITERIA FOR TRANSITION BETWEEN REGIMES

Criteria to determine the Regimes to be applied in the model are defined based on the stress intensity factor K_I. In **Regime I** the stresses are not sufficient to allow inelastic deformation (sliding or opening of the microcraks). This implies $K_I \leq 0$ at the tip of the cracks (K_I^{RII} or K_I^{RII}, since C and O are related to A and B). Therefore, based on equation s9 the criteria for **Regime I** is:

$$A\sigma + B\tau \leq 0 \tag{s30}$$

For the two regimes (II and III) undergoing inelastic deformation, K_I is positive and the transition between regimes is obtained by ensuring the continuity of conjugate strains ϵ^i and γ^i. The first invariant of the strain tensor corresponds to the opening of the microcracks, whereas the second invariant is related to the frictional sliding of the penny-shaped cracks. Under compressive loading, tensile deformation only occurs by opening of the wing cracks, whereas under **Regime III**, both penny shaped cracks and wing cracks opened due to normal tensile stress. As a consequence ϵ^i is smaller for compressive loading (Regime II) than for tensile loading (Regime III). Therefore, we are in **Regime II** when:

$$A\sigma + B\tau > 0 \quad \text{and} \quad (A^2 - C^2)\sigma + AB\tau > 0 \tag{s31}$$

and **Regime III** is reached for:

$$A\sigma + B\tau > 0 \quad \text{and} \quad (A^2 - C^2)\sigma + AB\tau < 0 \tag{s32}$$

S4 DYNAMIC CRACK GROWTH LAW

As underlined in section 2.3, for crack to grow, the dynamic micro-crack stress intensity factor, K_I^d (cf. section S1.2), must overcome the resistance of the material to fracturing, i.e. the fracture toughness K_{IC} determined by laboratory experiments only. For crack initiation $K_I^d > K_{IC}^D$, where K_{IC}^D is dynamic initiation toughness. Once the crack is initiated, the crack growth is controlled by the dynamic propagation toughness, $K_I^d = K_{IC}^d$.

S4.1 Dynamic Stress intensity Factor, K_I^d

Freund (1973) has shown that, for an unbounded body subjected to time independent loading, the stress intensity factor (K_I^d) for a dynamic growing crack tip ($v > 0$) can be expressed as the product of a crack-tip velocity dependent function, $k(v)$, time the value of the stress intensity factor at steady-state, $K_I(\boldsymbol{\sigma}, D)$:

$$K_I^d(v) = k(v)K_I(l) \quad \text{with} \quad k(v) \simeq \frac{1 - v/c_R}{\sqrt{1 - v/c_p}} \tag{s33}$$

where c_R and c_p correspond to the Rayleigh wave speed and the P-wave speed of the material respectively. The equation was derived for a single crack, we nonetheless used this relation as an approximation of the effective K_I^d for a unit volume containing N_v cracks.

S4.2 Dynamic Initiation toughness K_{IC}^D

Experiments performed for different rocks types have highlighted the loading rate dependency of K_{IC}^D(Wang et al. 2010, 2011; Zhang & Zhao 2013). A parameter to characterize the loading rate is:

$$\dot{K}_I = \frac{K_{I_{\text{cr}}}}{t_c} \tag{s34}$$

where $K_{I_{\text{cr}}}$ corresponds to the critical stress intensity factor at the instant of crack initiation (when it equals the fracture toughness) and t_c demotes the duration since the beginning of the loading to reach this critical value. Then the dynamic initiation toughness material property can be expressed as function of $\dot{K}_I$ time the its quasi-static limit K_{IC}^{ss}:

$$K_{IC}^D = f(\dot{K}_I)K_{IC}^{ss} \tag{s35}$$

where $f(\dot{K}_I) \geq 1$ takes into account the increase initiation toughness due to loading rate as observed in experimental data. Following Bhat et al. (2012) we assume in our model the subsequent relation :

$$K_{IC}^D = \left(1 + \frac{\dot{K}_I}{\alpha_K}\right) K_{IC}^{ss} \tag{s36}$$

where α_K is a given constant in our model that best fits the experimental data.

S4.3 Dynamic propagation toughness $K_{IC}^d(v)$

Rocks mechanics experiments have shown that the material resistance depends on the velocity at which the crack is propagating (Chen et al. 2009; Dai et al. 2010, 2011; Zhou & Aydin 2010; Zhang & Zhao 2013; Gao et al. 2015). Numerical study for mode III (Freund & Douglas 1982) and mode I (Deng & Rosakis 1991) crack growth under plane stress conditions, for elastic-perfectly plastic material, have shown that an increase in crack speed requires the monotonic increase of $K_{IC}^d(v)$ in order to keep satisfying a local critical crack opening displacement criterion. However, beyond a critical crack-tip velocity, it becomes more favorable for the crack to branch into one or more cracks ($K_{IC}^d(v)$ tends to infinite). This limiting speed, called the branching speed (v_m), is material-dependent and decreases with increasing material ductility. In our model, the crack-tip speed dependency of dynamic propagation toughness is taken into account with the following equation that well fit the experimental data (Bhat et al. 2012):

$$K_{IC}^d(v) = \left(\frac{1 + (v/v_m)^5}{\sqrt{1 - v/c_p}}\right) K_{IC}^{ss} \tag{s37}$$

Regardless of the material, the initation and propagation toughnesses always display the same trends. Therefore, in our model, we only need to provide the material properties corresponding to the branching speed (v_m) and the quasi-static fracture toughness K_{IC}^{ss}.

S4.4 Crack growth law

When the dynamic stress intensity factor satisfy the criteria $K_I^d > K_{IC}^D$, crack-tip starts propagating. For the crack to keep growing, K_I^d (equation s33) must equal K_{IC}^d. This leads to the following crack growth criterion:

$$\frac{1 - v/c_r}{\sqrt{1 - v/c_p}} K_I = \left(\frac{1 + (v/v_m)^5}{\sqrt{1 - v/c_p}}\right) K_{IC}^{ss} \tag{s38}$$

We therefore obtain a non linear equation for the crack-tip speed $v \equiv \mathrm{d}l/\mathrm{d}t$, which is solved using a Newton-Raphson method. In turn, $\mathrm{d}l/\mathrm{d}t$ is used in equation (3) to solve for damage evolution.

Parameter	Symbol	Equation
angle to σ_1 for microcracks	Φ	sec. 2.2
Damage variable	D	eq 2
Initial Damage variable	D_0	eq 1
stress intensity factor	K_I	eq s9, s15
dynamic stress intensity factor	K_I^d	eq s33
dynamic initiation toughness	K_{IC}^D	eq s36
dynamic fracture toughness	K_{IC}^d	eq s37
instantaneous wing-crack speed	$v \equiv \mathrm{d}l/\mathrm{d}t$	eq s38
stress tensor	σ_{ij} or $\boldsymbol{\sigma}$	eq s19, s22, s28
stress invariant	σ, τ	eq 8

Table S1. Parameters of the damage constitutive model

REFERENCES

Ashby, M. F. & Sammis, C. G., 1990. The damage mechanics of brittle solids in compression, *Pure and Applied Geophysics*, **133**(3), 489–521.

Bhat, H. S., Rosakis, A. J., & Sammis, C. G., 2012. A micromechanics based constitutive model for brittle failure at high strain rates, *Journal of Applied Mechanics-transactions of the Asme*, **79**(3), 031016.

Budiansky, B. & O'connell, R. J., 1976. Elastic moduli of a cracked solid, *International Journal of Solids and Structures*, **12**(2), 81–97.

Chen, R., Xia, K., Dai, F., Lu, F., & Luo, S., 2009. Determination of dynamic fracture parameters using a semi-circular bend technique in split hopkinson pressure bar testing, *Engineering Fracture Mechanics*, **76**(9), 1268–1276.

Dai, F., Chen, R., Iqbal, M., & Xia, K., 2010. Dynamic cracked chevron notched brazilian disc method for measuring rock fracture parameters, *International Journal of Rock Mechanics and Mining Sciences*, **47**(4), 606–613.

Dai, F., Xia, K., Zheng, H., & Wang, Y., 2011. Determination of dynamic rock mode-i fracture parameters using cracked chevron notched semi-circular bend specimen, *Engineering Fracture Mechanics*, **78**(15), 2633–2644.

Deng, X. M. & Rosakis, A. J., 1991. Dynamic crack-propagation in elastic - perfectly plastic solids under plane-stress conditions, *Journal of the Mechanics and Physics of Solids*, **39**(5), 683–722.

Deshpande, V. S. & Evans, A. G., 2008. Inelastic deformation and energy dissipation in ceramics: A mechanism-based constitutive model, *Journal of the Mechanics and Physics of Solids*, **56**(10), 3077–3100.

Freund, L. B., 1973. Crack-propagation in an elastic solid subjected to general loading .3. stress wave loading, *Journal of the Mechanics and Physics of Solids*, **21**(2), 47–61.

Freund, L. B. & Douglas, A. S., 1982. The influence of inertia on elastic plastic antiplane-shear crack-growth, *Journal of the Mechanics and Physics of Solids*, **30**(1-2), 59–74.

Gao, G., Yao, W., Xia, K., & Li, Z., 2015. Investigation of the rate dependence of fracture propagation in rocks using digital image correlation (dic) method, *Engineering Fracture Mechanics*, **138**(Complete), 146–155.

Kachanov, M., 1987. Elastic solids with many cracks: A simple method of analysis, *International Journal of Solids and Structures*, **23**(1), 23–43.

Perol, T. & Bhat, H. S., 2016. Micromechanics-based permeability evolution in brittle materials at high strain rates, *Pure and Applied Geophysics*, **173**(8), 2857–2868.

Thomas, M. Y., Bhat, H. S., & Klinger, Y., 2017. Effect of brittle off-fault damage on earthquake rupture dynamics, in *Fault Zone Dynamic Processes: Evolution of Fault Properties During Seismic Rupture*, vol. 227, pp. 255–280, eds Thomas, M. Y., Mitchell, T. M., & Bhat, H. S., John Wiley & Sons, Inc.

Wang, L., Hainzl, S., Sinan Özeren, M., & Ben-Zion, Y., 2010. Postseismic deformation induced by brittle rock damage of aftershocks, *Journal of Geophysical Research*, **115**(B10), B10422.

Wang, Q., Feng, F., Ni, M., & Gou, X., 2011. Measurement of mode i and mode ii rock dynamic fracture toughness with cracked straight through flattened brazilian disc impacted by split hopkinson pressure bar, *Engineering Fracture Mechanics*, **78**(12), 2455–2469.

Zhang, Q. & Zhao, J., 2013. Effect of loading rate on fracture toughness and failure micromechanisms in marble, *Engineering Fracture Mechanics*, **102**, 288–309.

Zhou, X. & Aydin, A., 2010. Mechanics of pressure solution seam growth and evolution, *Journal of Geophysical Research*, **115**(B12), B12207.

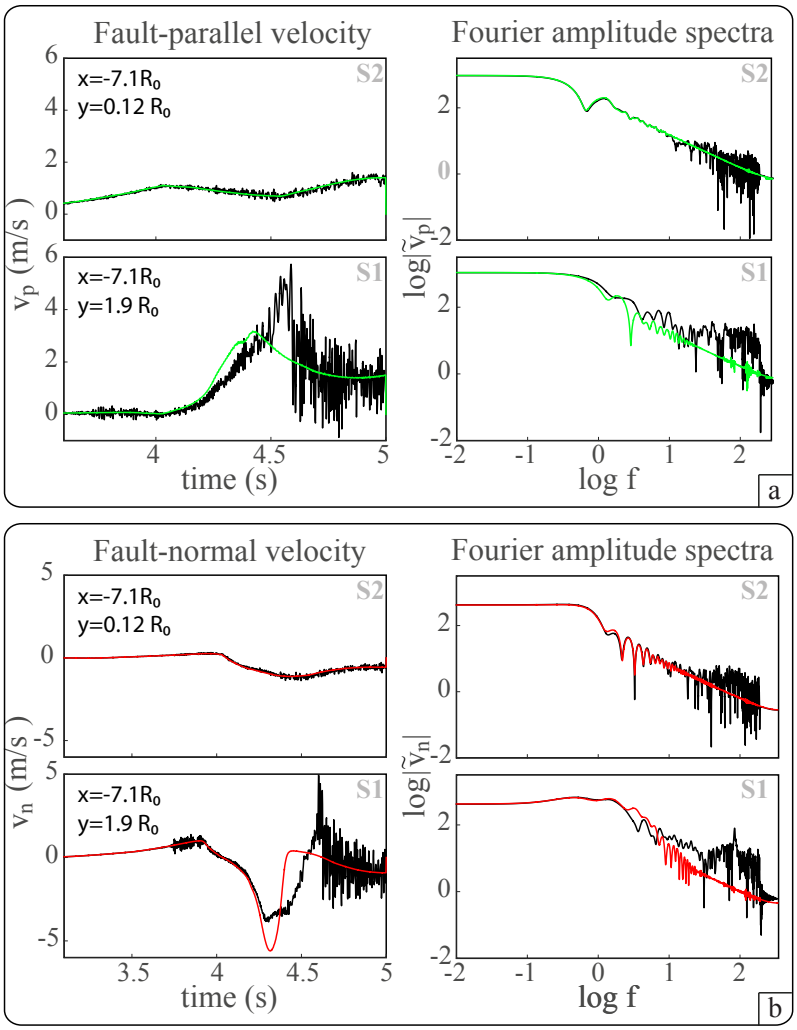

Figure S1. Synthetic seismograms of fault-parallel (a) and fault-normal (b) velocities with the corresponding Fourier amplitude spectra (FAS). Black curves correspond to the dynamic simulation with homogeneous elastic properties but different initial damage (case 1, Fig. 2). Colored curves correspond to a simulation with the same parametrization but within a pure elastic medium. "x" and "y" coordinates give the location of the synthetic seismometers. Modified from (Thomas et al. 2017).